Scripta Materialia 116 (2016) 67–70

Contents lists available at ScienceDirect

Scripta Materialia

journal homepage: www.elsevier.com/locate/scriptamat

Regular Article

Tungsten carbide is more oxidation resistant than tungsten when processed to full density

Samuel A. Humphry-Baker *, William E. Lee

Department of Materials, Imperial College London, Prince Consort Road, London SW7 2BP, United Kingdom

ARTICLE INFO

Article history:
Received 27 November 2015
Accepted 4 January 2016
Available online xxxx

Keywords:
Tungsten carbide
Tungsten
Oxidation
Kinetics
Porosity

ABSTRACT

Previous studies report that WC oxidises in air more readily than W. However, systematic thermogravimetric studies reveal considerably slower oxidation kinetics in WC samples, which outperform previous measurements by 1–2 orders of magnitude. By combining X-ray diffraction and electron microscopy, the enhanced stability in WC is explained by a dense interlayer of sub-stoichiometric WO_3, approximately 10 μm in thickness, which forms adjacent to the substrate/oxide interface. The faster oxidation kinetics from previous studies are explained by the comparatively low densities of samples used.

Tungsten and its carbides have excellent high temperature properties such as strength, stiffness, and thermal conductivity. Combined with their relatively low cost, they are being developed for many technologies requiring extreme environments, such as nuclear fusion reactors. In particular, W is a leading candidate for structural and armour components [1], while WC shows promise for shielding in compact spherical reactors [2]. The drawback of these materials is their susceptibility to oxidation at relatively modest temperatures [3], which can present major safety issues; e.g. under accidental conditions in a nuclear fusion reactor, where oxidation could release tungsten oxide vapours and transmutation products [4].

The kinetics of tungsten oxidation have been reviewed extensively [5–7], and can generally be categorised by three temperature regimes: From about room temperature to 500 °C, a protective bluish oxide scale of substoichiometric WO_3 forms, leading to parabolic oxidation kinetics [5,7–9]. Above about 500 °C, a yellow WO_3 scale begins to grow, whilst retaining the protective blueish interior below [5,9]. The outer layer is generally highly cracked and thus unprotective [10,11], therefore linear kinetics are generally observed [5–7,12,11]. The parabolic-to-linear transition is time-dependent as cracking-onset is dependant on scale thickness [5]. Finally above 1000 °C, volatilisation of the WO_3 scale becomes significant, eventually leading to overall mass loss of the sample [10].

The picture for pure WC is less clear, despite much work on composites such as WC–Co [13–16]. The oxidation kinetics of WC were reported to be faster than W – by about an order of magnitude – e.g. in the range 700–1000 °C [12] and 700–900 °C [17]. Poor carbide performance was explained by formation of CO_2 gas at the interface [12], inducing excessive porosity and scale cracking. More recent evidence has cast doubt over these initial studies; at least in the range 0–500 °C, where thicker oxide scales were reported on W [18,19]. On a related contradiction, it is frequently cited that pure WC oxidises faster than WC–Co [17,20,21], but increasing Co content is generally found (although not always [16]) to increase the oxidation rate [13,15]. Thus, the literature is inconsistent, and what is more, no systematic comparison exists over a wide temperature range.

We report the oxidation kinetics of pure W and WC between 600 and 1000 °C. Counter to previous studies [12,17], we find the rate of oxidation in our WC samples is a factor of 10 or more slower. This discrepancy is explained by formation of a dense protective off-stoichiometric oxide interlayer in our samples, which would have been prevented from forming in previous studies where samples were highly porous.

Tungsten rod (Alpha Aesar, 99.7% purity), and tungsten carbide pellet (SPS Syntex, Ltd.), were cut into samples of about 6 × 3 × 3 mm, i.e. about 1 g each. For each oxidation experiment, samples were loaded into an alumina crucible inside a STA 449 F5 Jupiter Thermogravimetric Analyser (TGA). Fig. 1 shows the mass change and temperature profile during a typical experiment at 1000 °C. The sample was heated to the set-point in high purity argon, and held isothermally for 1 h. For lower temperatures, longer dwell times of about 2, 3, 10 and 15 h were used at 900, 800, 700 and 600 °C respectively. Once the temperature stabilised, synthetic air (80% N_2; 20% O_2) was flowed over the sample at 100 ml/min for the test duration, after which the flow gas was switched back to Ar and cooled. The mass gain signal in Fig. 1 shows a stable and repeatable increase, which initiates at the instant the air is flowed over the sample.

* Corresponding author.
E-mail address: shumphry@ic.ac.uk (S.A. Humphry-Baker).

http://dx.doi.org/10.1016/j.scriptamat.2016.01.007

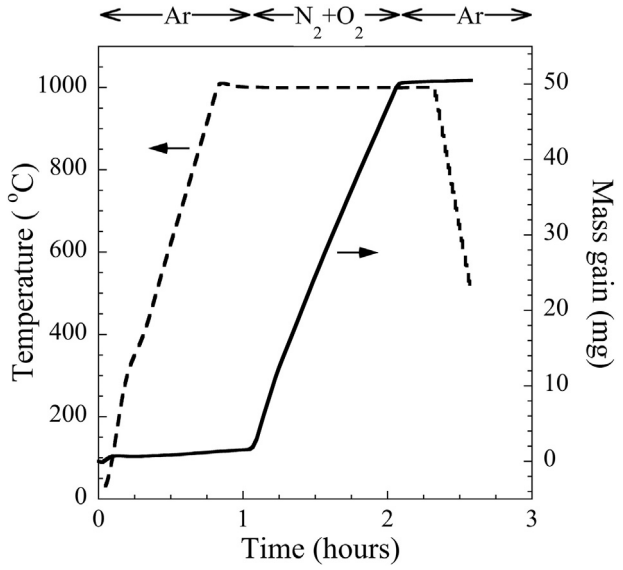

Fig. 1. Overview of a typical TGA experiment, showing the temperature profile, and injection of synthetic air once the set-point is reached.

To relate the mass gain signal to a true oxidation rate, the instantaneous WC-substrate surface area must be known. The initial area of each specimen was calculated from its dimensions (as measured using a micrometre of accuracy ±0.002 mm), from which the reduction in area of the sample was corrected for by assuming firstly that the WC substrate (of density 15.5 g/cm^3) recedes isotropically in all directions, and secondly, that it is fully converted to WO_3 (i.e. 195.8 → 231.8 g/mol), with carbon dioxide gas being released into the vapour phase. A similar calculation was performed for W. The resultant oxidation rates are plotted in Fig. 2(a) for pure W at various temperatures. The plot is on a log–log scale, and thus the gradient of the line reveals the nature of the kinetic trend. At all temperatures, the signals tend toward a gradient of $m = 1$ at long times, which is indicative of linear oxidation kinetics, as is often reported for W in this temperature regime. The rate constant at each temperature, as calculated from the straight-line fit, is plotted as a function of inverse temperature in Fig. 2(b), alongside similar results for pure WC, where again linear kinetics are observed. The data can be fit with an Arrhenius-law, from which the apparent activation energy is lower for WC vs. W (80 and 130 kJ/mol respectively). Correspondingly, WC oxidises faster at low temperatures, but slower at high temperatures, with a cross-over occurring around 800–900 °C. The rate constants from Webb et al. [12] (which broadly agree with Kieffer and Kolbl [17]) are superimposed on the plot — as determined from linear fits to reported oxidation curves. Our methods are nominally the same, and as expected, our rate constants for W appear to agree. However there is stark disagreement for WC; our measured rates are about an order of magnitude lower.

To further elucidate the discrepancy between this study and the literature [12,17], the structural evolution in the WC oxide layer is now considered in detail. Fig. 3 depicts the change in the oxidised WC surfaces at increasing temperature: Part (a) shows a series of X-ray Diffraction (XRD) patterns from the oxidised WC surfaces, which were acquired on a Panalytical Pro instrument at a rate of 2.5°/min, and matched to ICDD Powder Diffraction Files (PDFs). A gradual structural transition is detected: (i) orthorhombic WO_3 (PDF 20-1324) at 600 °C; (ii) triclinic WO_3 (32–1395) at intermediate temperatures; and (iii) tetragonal WO_2 (35–0791) at 1000 °C. Part (b) shows images of these oxide surfaces, taken on a JSM 6010 scanning electron microscope (SEM) in secondary electron (SE) mode. At low temperatures the scales are highly cracked, however, there was a general trend across all samples toward less cracking in the scale at higher temperatures; at 700 °C the cracks are spaced only about 50 μm apart, at 800 °C they have perhaps a 200 μm separation, and at 900 °C they are barely visible. The driving force for crack growth is likely the large ratio between the theoretical density of carbide and the oxide, $\rho_{carbide}/\rho_{oxide} = 2.2$, leading to compressive stresses in the plane of the pellet surface. The lack of cracking at high temperature suggests that the volume expansion can be accommodated by plastic deformation; at 1000 °C the oxide layer is at about 0.73 T_m, i.e. above the threshold for diffusive creep processes in oxides — which typically begin in oxides on the order of 0.7 T_m [22]. The lack of cracking in the outer scales at high temperatures suggests that some other short-circuit path, such as open porosity, must account for its unprotective nature.

To explain this structural transition, samples were sectioned normal to the surface by manual polishing to reveal the phases present below the surface. Between 600 °C and 800 °C the scales are homogeneously WO_3 throughout, however at 900 °C and 1000 °C, sectioning revealed three different phases. Fig. 4 shows the structure at 1000 °C in detail,

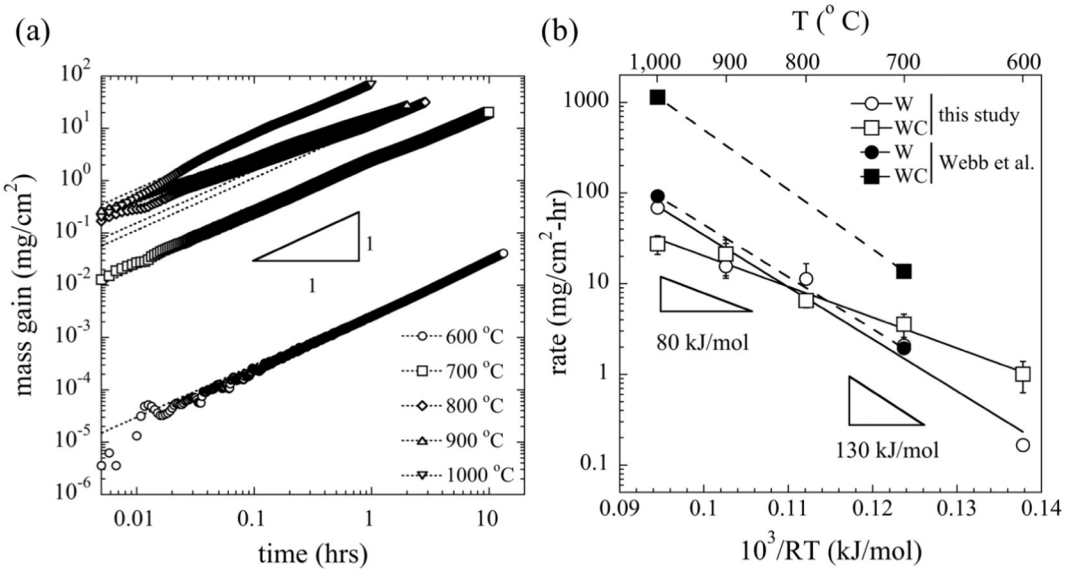

Fig. 2. Oxidation kinetics of W and WC. (a) shows linear oxidation kinetics for W. The rate constants are plotted (open circles) in (b) along with results for WC (open squares), as a function of inverse temperature, yielding activation energies of 130 and 80 kJ/mol respectively. Compared to the literature (closed symbols), our rate constants agree relatively well for W, however those for WC are dramatically lower. Error bars represent largest deviation in slope from fits to final or initial 10% of data.

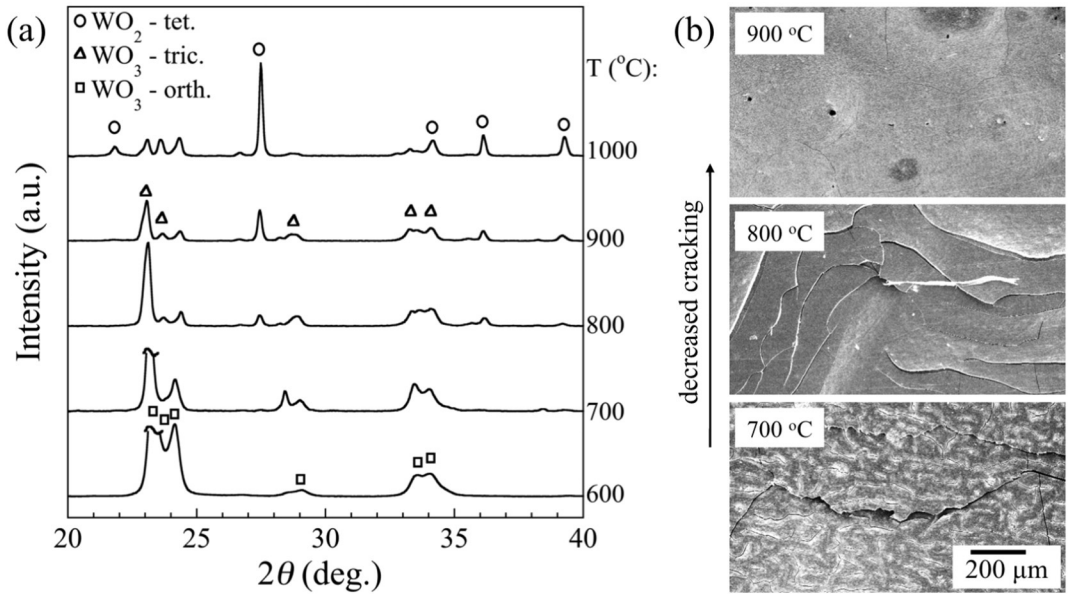

Fig. 3. Evolution in WC oxide surface with temperature: (a) XRD patterns of the oxide surface show a clear transition — orthorhombic WO_3 at low temperatures through triclinic WO_3, to tetragonal WO_2 at high temperatures. (b) The oxide structure is increasingly cracked at lower temperatures.

which is representative of the sample at 900 °C as well. Part (a) shows a cross-sectional image taken in SE mode. Part (b) shows XRD patterns from successive depths, which are indicated by the arrows in (a). The patterns show that the dark brown monoclinic WO_2 is confined to the outer surface region; with yellow triclinic WO_3 making up the bulk of the scale; and at the inner surface – i.e. adjacent to the carbide/oxide interface – is a bluish phase with a diffraction pattern best fitted by the sub-stoichiometric monoclinic structures: $WO_{2.9}$ (PDF 5-0386) or $WO_{2.8}$ (5–0387).

To clarify the role of the bluish sub-stoichiometric interlayer, it was imaged at higher resolution under back-scattered electron mode, as shown in the inset of Fig. 4(a). The interlayer is shown to be pore-free, with the material above increasingly porous; the average scale porosity can be estimated from the oxide thickness of about 200 μm, which would equate to a volume of about 0.019 cm^3 in a 5.1 × 3.5 × 3.5 mm pellet. Based on a measured mass gain of 11.6 mg, the density of the oxide layer would be 3.9 g/cm^3, or about 55% of theoretical for WO_3 (7.16 g/cm^3). Such a high pore fraction, well above the percolation

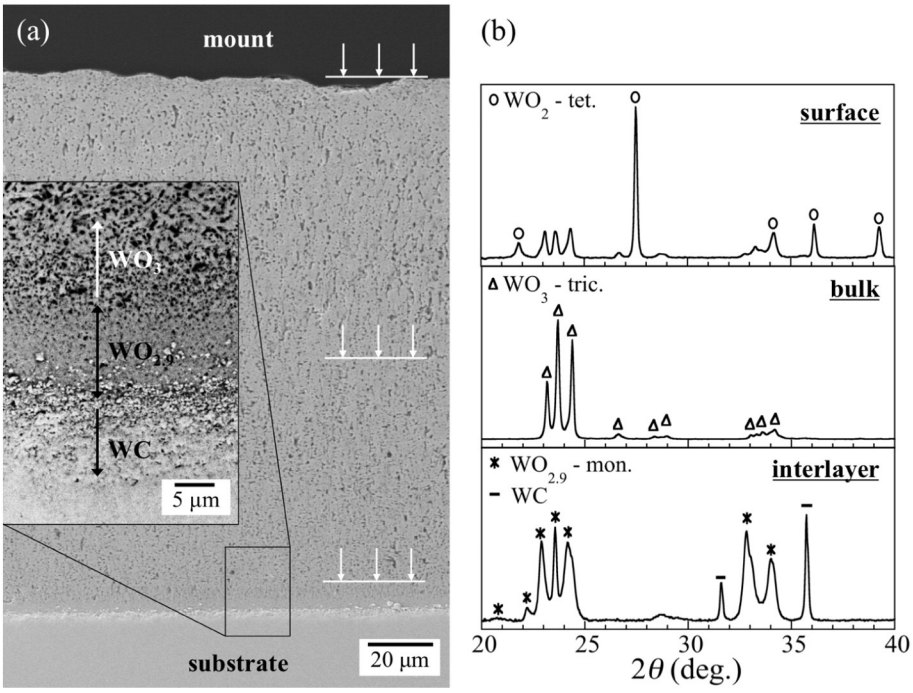

Fig. 4. A dense interlayer forms at the substrate interface after heating to 1000 °C. (a) SEM cross section in SE mode shows a porous oxide thickness of about 200 μm in thickness; the inset taken in BSE mode shows a dense and pore free interlayer at the carbide/oxide interface, with a thickness of about 5–10 μm. (b) XRD patterns, taken from sections at depths indicated by the arrows, show the interlayer is an off-stoichiometric monoclinic $WO_{2.9}$/$WO_{2.8}$.

threshold, would allow easy transport of oxygen to the surface. Porosity in the oxide layer can arise from formation of gaseous CO_2 according to a non-preferential oxidation reaction:

$$WC + 2.5\ O_2 \rightarrow WO_3 + CO_2, \quad (1)$$

which has been proposed previously [12], based on previous observation of CO_2 formation and the fact that the WC phase has a narrow range of C stoichiometry, thus preventing any selective oxidation of tungsten. The lack of scale cracking at high temperatures, in combination with the interconnected open pore structure and the observation of linear kinetics in the thermogravimetry studies, confirms that the main oxide scale is non-protective and thus oxygen transport through it does not limit the rate of oxidation.

On the other hand, the pore-free nature of the sub-stoichiometric interlayer located at the carbide/oxide interface suggests that it plays a protective role. Although a sub-stoichiometric WO_{3-x} layer would contain excess oxygen vacancies, and thus allow faster diffusion than otherwise identical stoichiometric WO_3 [23], the fact that no cracking, delamination, or rupture was found, indicates that it would provide a significant barrier for oxygen diffusion, as is proposed for sub-stoichiometric interfacial films on pure W [5,7–9]. The interlayer remains at a thickness of about 10 μm, regardless of the oxidation time, presumably because it is limited by pore growth under the pressure of CO_2 gas. Such growth can proceed via creep deformation at these temperatures [22] and once significant pore connectivity is obtained, its role as diffusion barrier will be lost. Thus we envisage a steady state; whereby new interlayer is formed at the leading edge by the reaction of Eq. (1), and old interlayer is lost at the trailing edge by void coalescence. In such a way the interlayer thickness will remain constant, which is consistent with observations of linear mass-gain kinetics, despite its protective nature.

We now turn our analysis to explaining the stark differences in oxidation rate of WC between our results and those in the literature. Methods used in both studies are directly comparable, the only difference being the relative densities of the WC specimens; in our case, the density was measured using the Archimedes method to be 15.5 g/cm^3, i.e. >99% theoretical density; whereas the densities of Webb et al. [12] were only 90%. Pores are well known to dramatically reduce the strength of ceramics [24], and the same is expected for oxide scales [25]. We envisage that pores would disrupt the otherwise protective nature of the sub-stoichiometric interlayer, by premature interlayer delamination or cracking [26]. Indeed, a link between higher porosity and accelerated oxidation has been experimentally observed in graphite [27], and in numerical calculations on tungsten [28] — the latter of which predicted an order of magnitude increase in oxidation rate in porous material.

In summary, when WC is processed to full density, the rate of oxidation at high temperatures is decreased dramatically compared to highly porous material. As a result, WC can outperform W at temperatures above about 900 °C. The result not only has implications for materials selection in many high temperature structural applications where protecting against oxidation is desirable, but also for the development of cemented carbide composites, where the fundamentals of oxidation resistance remain unclear. More broadly, the deleterious effect of porosity that this study highlights can provide guidance for future research in non-oxide ceramics, where due to their high melting point and need to process in controlled inert or reducing atmospheres it is often difficult to process to full density.

Acknowledgement

The authors would like to thank the EPSRC program grant (EP/K008749/1) Materials Systems for Extreme Environments (XMat) and Tokamak Energy Ltd. for financial support.

References

[1] M. Kaufmann, R. Neu, Fusion Eng. Des. 82 (2007) 521–527.
[2] C.G. Windsor, J.G. Morgan, P.F. Buxton, Nucl. Fusion 55 (2015) 023014.
[3] A. Gromov, Y.-S. Kwon, P.-P. Choi, Scr. Mater. 52 (2005) 375–380.
[4] F. Koch, H. Bolt, Phys. Scr. 2007 (2007) 100.
[5] V.Y.E. Ivanov, (1969).
[6] G.D. Rieck, Tungsten and Its Compounds, Pergamon Press, 1967.
[7] E. Lassner, W.-D. Schubert, Tungsten, Springer US, Boston, MA, 1999.
[8] E.A. Gulbransen, W.S. Wysong, Trans. AIME 175 (1948) 611–627.
[9] E.A. Kellett, S.E. Rogers, J. Electrochem. Soc. 110 (1963) 502–504.
[10] E.A. Gulbransen, K.F. Andrew, F.A. Brassart, J. Electrochem. Soc. 111 (1964) 103–109.
[11] S.C. Cifuentes, M.A. Monge, P. Pérez, Corros. Sci. 57 (2012) 114–121.
[12] W.W. Webb, J.T. Norton, C. Wagner, J. Electrochem. Soc. 103 (1956) 112–117.
[13] F. Lofaj, Y.S. Kaganovskii, J. Mater. Sci. 30 (1995) 1811–1817.
[14] L. Del Campo, R.B. Pérez-Sáez, L. González-Fernández, M.J. Tello, Corros. Sci. 51 (2009) 707–712.
[15] S.N. Basu, V.K. Sarin, Mater. Sci. Eng. A 209 (1996) 206–212.
[16] J.M.S.M. Aristizabal, Corros. Sci. 53 (2011) 2754–2760.
[17] R. Kieffer, F. Kölbl, Z. Für Anorg. Chem. 262 (1950) 229–247.
[18] Y. Jiang, J.F. Yang, R. Liu, X.P. Wang, Q.F. Fang, J. Nucl. Mater. 450 (2014) 75–80.
[19] A. Warren, A. Nylund, I. Olefjord, Int. J. Refract. Met. Hard Mater. 14 (1996) 345–353.
[20] J.G. Carla Barbatti, Int. J. Refract. Met. Hard Mater. 27 (2009) 768.
[21] V.B. Voitovich, V.V. Sverdel, R.F. Voitovich, E.I. Golovko, Int. J. Refract. Met. Hard Mater. 14 (1996) 289–295.
[22] H. Hahn, R.S. Averback, J. Am. Ceram. Soc. 74 (1991) 2918–2921.
[23] V.K. Sikka, C.J. Rosa, Corros. Sci. 20 (1980) 1201–1219.
[24] R.W. Rice, J. Mater. Sci. 19 (1984) 895–914.
[25] M.M. Nagl, W.T. Evans, J. Mater. Sci. 28 (1993) 6247–6260.
[26] P. Hancock, J.R. Nicholls, Mater. Sci. Technol. 4 (1988) 398–406.
[27] D. Chen, Z. Li, W. Miao, Z. Zhang, Mater. Trans. 53 (2012) 1159–1163.
[28] D. Berman, J. Appl. Phys. 38 (1967) 780–783.